

## Electronic structure of $\text{TiO}_2\text{:Ru}$

Keith M. Glassford and James R. Chelikowsky

*Department of Chemical Engineering and Materials Science, Minnesota Supercomputer Institute,  
University of Minnesota, Minneapolis, Minnesota 55455*

(Received 14 December 1992)

We present *ab initio* electronic structure calculations of Ru-doped  $\text{TiO}_2$  using a supercell geometry. Our results show three Ru-induced defect states occurring within the fundamental  $\text{TiO}_2$  band gap with a center of mass  $\sim 1$  eV above the O  $2p$  manifold in agreement with absorption and photoelectrochemical experiments. These midgap states were found to be localized on the Ru atoms with  $t_{2g}$ -like symmetry.

Significant advances have been made both theoretically and experimentally in our ability to modify the electronic properties of semiconductors through doping and/or alloying. While “band-gap engineering” is well known in the semiconductor industry, its application to transition-metal oxides is in a more primitive stage. This fact notwithstanding, the electronic modification of these materials is becoming increasingly important for a number of technological applications. Unlike semiconductors, few theoretical investigations have been performed for transition-metal oxides. Traditionally, oxides have been one of the most difficult classes of solids upon which to perform “first-principles” pseudopotential calculations, owing to the localized nature of the transition-metal  $d$  and O  $2p$  valence wave functions.<sup>1,2</sup> However, with the recent advances in techniques for generating “soft-core” transferable pseudopotentials,<sup>3,4</sup> and fast iterative diagonalization techniques,<sup>5</sup> we are now in a position to handle these complex systems from first principles.

As a first step toward “band-gap engineering” for transition-metal oxides using *ab initio* calculations, we have chosen to study the  $\text{Ru}_x\text{Ti}_{1-x}\text{O}_2$  system, owing to its use in energy-storage and conversion processes,<sup>6–8</sup> in the photocatalytic treatment of waste water,<sup>9</sup> in antichalking agents in the paint and polymer industry,<sup>10</sup> as a catalyst in the photomethanation of carbon dioxide,<sup>11</sup> and as an electrocatalyst in the chloralkali industry.<sup>12,13</sup> These applications depend upon the transfer of electrons (holes) from the conduction (valence) band to a reactant molecule or electrolyte after the electroexcitation/photoexcitation process. The reaction pathways at the surface are often complex, and in many instances remain unknown. An understanding of the bulk electronic properties for these mixed oxide systems, and the location of impurity states, will aid in the design of better catalysts and electro-optic devices. An example of the impact of “band-gap engineering” in transition-metal oxides is illustrated by the production of  $\text{H}_2$  through band-gap illumination of  $\text{TiO}_2$  electrodes.<sup>6</sup> The difficulty with this process, however, lies in the 3.05-eV band gap<sup>14</sup> found in pure  $\text{TiO}_2$ . This large gap results in photon absorption near the uv region of the spectrum where solar photon fluxes are small. By doping  $\text{TiO}_2$ , it is hoped that the absorption spectrum may be shifted to longer wavelengths through the formation of induced states within the funda-

mental band gap, thereby making  $\text{TiO}_2$  an attractive material for energy-storage and conversion processes.

Although the electronic properties of  $\text{TiO}_2$  have been extensively studied in the literature,<sup>1</sup> and those of  $\text{RuO}_2$  to a lesser extent,<sup>2</sup> little is known theoretically about the  $\text{Ru}_x\text{Ti}_{1-x}\text{O}_2$  system. Here we present *ab initio* calculations performed within the local-density approximation for the quasibinary  $\text{Ru}_x\text{Ti}_{1-x}\text{O}_2$  oxide, using a plane-wave basis and “soft-core” pseudopotentials.<sup>3</sup> We have recently shown this methodology to give good results<sup>1,2</sup> for the electronic, structural, and optical properties of the end-member oxides  $\text{TiO}_2$  and  $\text{RuO}_2$ . Our Ti, Ru, and O pseudopotentials were generated by the method of Troullier and Martins,<sup>3</sup> as previously described.<sup>1,2</sup> Here we will focus upon the symmetry and location of Ru-induced impurity states relative to the valence-band edge of crystalline  $\text{TiO}_2$ , by examining the  $\text{Ru}_x\text{Ti}_{1-x}\text{O}_2$  system as  $x \rightarrow 0$ .

We have performed total-energy pseudopotential calculations for ideal  $\text{Ru}_x\text{Ti}_{1-x}\text{O}_2$  solid solutions at  $x = 0, \frac{1}{24}, \frac{1}{4}, \frac{1}{2}, \frac{3}{4},$  and 1. We employed supercells with the appropriate number of Ru atoms substituted for Ti. At  $x = \frac{1}{2}$  we use a  $1 \times 1 \times 1$  cell, at  $x = \frac{1}{4}$  and  $\frac{3}{4}$  a  $1 \times 1 \times 2$  supercell, and at  $x = \frac{1}{24}$  a  $2 \times 2 \times 3$  supercell. While lattice rearrangement is possible, we do not expect any significant modifications from the tetragonal symmetry of our supercells. In fact, solid solution behavior might be expected for  $0 < x < 1$ , as both  $\text{Ru}^{4+}$  and  $\text{Ti}^{4+}$  have similar ionic radii, electronegativities, and both oxides occur in the rutile structure with similar lattice constants. At each concentration, excluding  $\frac{1}{24}$  which will be discussed below, we have minimized the total energy with respect to the tetragonal lattice constants  $a$  and  $c$ , and the atomic positions of the Ru, Ti, and O atoms. The number of special  $\mathbf{k}$  points was increased until convergence in the total energy of 0.05 eV per formula unit of  $\text{Ru}_x\text{Ti}_{1-x}\text{O}_2$ , or better, was obtained. For  $x = 0$ , we have used one special  $\mathbf{k}$  point, eight for  $x = \frac{1}{4}, \frac{1}{2}, \frac{3}{4}$ , and six points for  $x = 1$ . Calculations were performed with a 64-Ry plane-wave cutoff, resulting in total energies which were converged to 0.05 eV/atom or better for the end-member oxides.

In Fig. 1, we show the resulting density of states (DOS) for  $x = \frac{1}{4}$  along with the  $\text{TiO}_2$  and  $\text{RuO}_2$  end-member oxides. The DOS was calculated using the analytic tetrahedron method,<sup>15</sup> employing the self-consistent solu-

tion at 126  $\mathbf{k}$  points in the irreducible Brillouin zone. The DOS for  $\text{TiO}_2$  and  $\text{RuO}_2$  have been discussed previously,<sup>1,2</sup> and will be mentioned only briefly in connection with the mixed oxide system. The Fermi energy has been taken as the energy zero in each panel, while occupied states are indicated by shading. Valence-band states between  $-9$  and  $-1$  eV are predominantly O  $2p$  states, while those greater than  $-1$  eV are predominantly Ti  $3d$  and Ru  $4d$  states in analogy with the  $t_{2g}$  and  $e_g$  states of an octahedrally coordinated transition-metal ion in the presence of a crystal field. For  $0 < x < 1$ , the width of the O  $2p$  manifold monotonically increases with  $x$ , resulting in a separation of  $\sim 1$  eV between end members, while the separation between the top of the O  $2s$  (not shown) and the bottom of the O  $2p$  manifold monotonically decreases by  $\sim 1$  eV between end members. At these concentrations, we find the heat of mixing for the ordered oxides to be positive, i.e., unstable, in agreement with experiment.<sup>17</sup>

The substitution of Ru for Ti results in an attractive

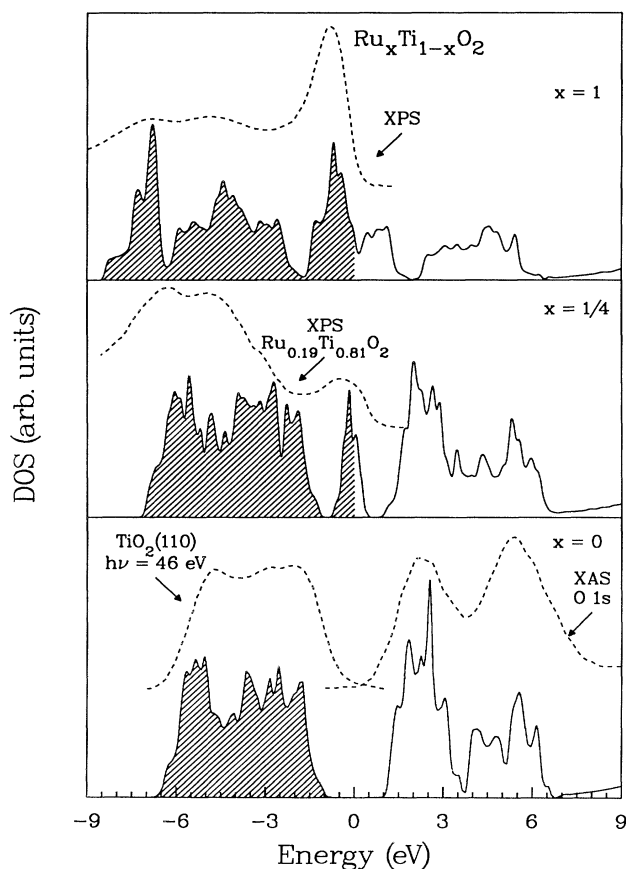


FIG. 1. Density of states for  $\text{Ru}_x\text{Ti}_{1-x}\text{O}_2$  for various Ru concentrations compared to experimentally determined spectra (Refs. 19 and 23–25). The Fermi energy has been taken as the energy zero while shading indicates occupied states. Theoretical results have been convoluted with a Gaussian of half-width at half maximum of 0.075 eV to account for finite sampling errors.

potential for the additional electrons originating from the atomic Ru  $4d$  states. This attractive potential subsequently lowers states in the  $t_{2g}$ - $e_g$  manifold. For  $x \ll 1$ , one expects localized Ru  $4d$  states in the vicinity of the  $\text{TiO}_2$  fundamental gap, as experimentally observed<sup>16</sup> for V, Cr, Fe, and Mn dopants in  $\text{TiO}_2$ . At higher Ru concentrations, these localized states will tend to overlap due to the decreasing Ru-Ru distance and eventually lead to metallic character as the  $t_{2g}$  and  $e_g$  complexes are pulled down toward the O  $2p$  manifold, as seen in Fig. 1. For  $x = \frac{1}{4}$ , the Ru-induced impurity states are clearly seen to occupy the fundamental  $\text{TiO}_2$  band gap. The width of the impurity complex is  $\sim 1$  eV and is separated from the valence-band and conduction-band edges by a gap of  $\sim 0.5$  eV. From our band-structure calculations, we find this midgap feature to be composed of three states. As the charge state of Ru in  $\text{Ru}_x\text{Ti}_{1-x}\text{O}_2$  has been experimentally determined<sup>17,18</sup> from Mössbauer absorption spectra to be almost exclusively  $\text{Ru}^{4+}$  ( $4d^4$ ), one expects two filled defect bands (excluding spin) associated with the substitutional Ru. Overall, the DOS for the  $x = \frac{1}{4}$  binary oxide remains similar to that of the undoped crystal shown in the bottom panel of Fig. 1. Recent x-ray-photoelectron spectroscopic experiments have been performed for electrochemically active  $\text{RuO}_2$ - $\text{TiO}_2$ /Ti overlayers<sup>19</sup> containing  $\sim 20$  mol %  $\text{RuO}_2$ . A comparison between our theoretical results and the experimental XPS spectra of the  $\text{Ru}_{0.19}\text{Ti}_{0.81}\text{O}_2$  films is given in the center panel of Fig. 1. Overall, our theoretical valence-band features are in good agreement with the experimental spectra given the morphological and stoichiometric differences. As the concentration is increased, we find the Ru midgap states overlap with the  $t_{2g}$ - $e_g$  manifold at  $x \sim 0.4$ .

The exact location of Ru states, however, is difficult to assess in the case of  $x = \frac{1}{4}$ , as the width of the defect complex is  $\sim 60\%$  of the  $\text{TiO}_2$  band gap. Further, these Ru-induced states become difficult to probe experimentally, owing to surface and defect states lying in the fundamental gap.<sup>20,18</sup> The variability of the transition-metal valence charge leads to further difficulties in determining whether these states are donors or acceptors when optical experiments are employed. Theoretically, the position of these defect states is determined by calculating the electronic structure of the alloy in the infinitely dilute limit. For semiconductors, however, the problem is difficult to treat using a supercell geometry, as defect-defect interactions lead to a significant dispersion of these states unless very large supercells are employed. Owing to the localized nature of the transition-metal  $d$  and O  $2p$  wave functions, much smaller supercells may be used in comparison to, e.g., Si:P. As the Ru-induced states have already localized in the band gap by  $x = \frac{1}{4}$ , as seen in Fig. 1, we have modeled the  $\text{TiO}_2\text{:Ru}$  system by using a Ru concentration of  $x = \frac{1}{24}$  with a  $2 \times 2 \times 3$  supercell containing 72 atoms. At this concentration, the minimum Ru-Ru separation is a factor of 2 larger than  $x = \frac{1}{4}$ . As in the case of  $\text{TiO}_2$ , one special  $\mathbf{k}$  point was used to sample the charge density. The lattice constants for the tetragonal supercell were based on  $\text{TiO}_2$ , as experimental x-ray-diffraction ex-

periments<sup>21</sup> for  $x \leq 0.02$  found differences of only 1–3 % from those of  $\text{TiO}_2$ . To ease the computational burden, the plane-wave cutoff was reduced from 64 to 40 Ry, as the band structure converges much faster than the total energy. We have tested the 40-Ry cutoff for crystalline  $\text{TiO}_2$ , finding relative shifts in the band structure on the order of 0.1 eV.

To estimate the location of Ru-induced impurity bands relative to the top of the O  $2p$  manifold for  $\text{TiO}_2\text{:Ru}$ , band-structure calculations were performed for  $x = \frac{1}{24}$ . In Fig. 2, we show the three Ru-induced gap states along various high-symmetry directions of the tetragonal Brillouin zone (BZ), where the Fermi energy has been taken as the energy zero. In this figure, the filled O  $2p$  valence states are indicated by shading while only the bottom of the conduction bands are shown. The bandwidth of the Ru-induced defect states was found to be 0.37 eV while the difference between the top of the O  $2p$  valence-band states and the bottom of the Ti  $t_{2g}$  states remains essentially unchanged from the local-density-approximation (LDA) value of 2.02 eV for pure  $\text{TiO}_2$ . Comparing the bandwidth at a doping of  $x = \frac{1}{4}$  of 1.2 eV, the defect-induced bandwidth at  $x = \frac{1}{24}$  has decreased by a factor of approximately 3 upon doubling the minimum Ru-Ru separation. The center of gravity of the Ru-induced complex is approximately 1 eV above the O  $2p$  manifold. Ultraviolet photoelectron spectroscopic experiments performed by Triggs<sup>18</sup> for single crystals doped with 2% Ru

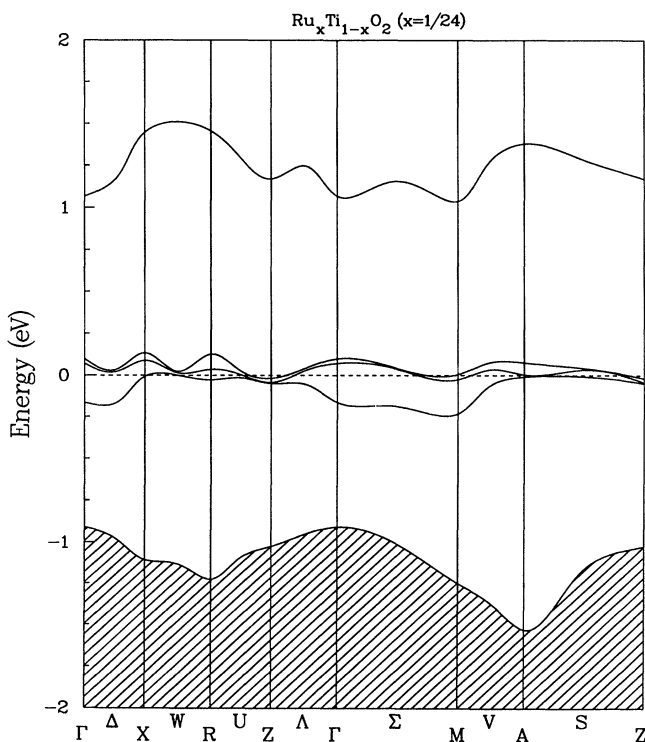


FIG. 2. The band structure of  $\text{Ru}_x\text{Ti}_{1-x}\text{O}_2$  at  $\frac{1}{24}$  along various high-symmetry directions. The Fermi energy has been taken as the energy zero.

resulted in a valence band similar to the undoped  $\text{TiO}_2$  spectra. While this Ru doping is close to our Ru concentration of  $x = \frac{1}{24}$ , variations in surface stoichiometry and a large depletion-layer width make it difficult to assign features to bulk spectra.<sup>18</sup> These experiments did, however, reveal a shift in the valence-band edge into the fundamental  $\text{TiO}_2$  band gap, corresponding to occupied Ru  $4d$  impurity states. A more direct comparison of the location of the impurity-induced Ru states to experiment is obtained by Triggs<sup>18</sup> from single-crystal optical-absorption spectra. For crystals doped with 2% Ru, a shift in the fundamental absorption edge from 3.05 (Ref. 14) to 1.85 eV was observed. Gutiérrez and Salvador<sup>22</sup> have performed photoelectrochemical experiments on  $\text{Ru}_{0.03}\text{Ti}_{0.97}\text{O}_2$  single crystals, revealing two distinct transitions. The first transition occurs at 3.2 eV, correspond-

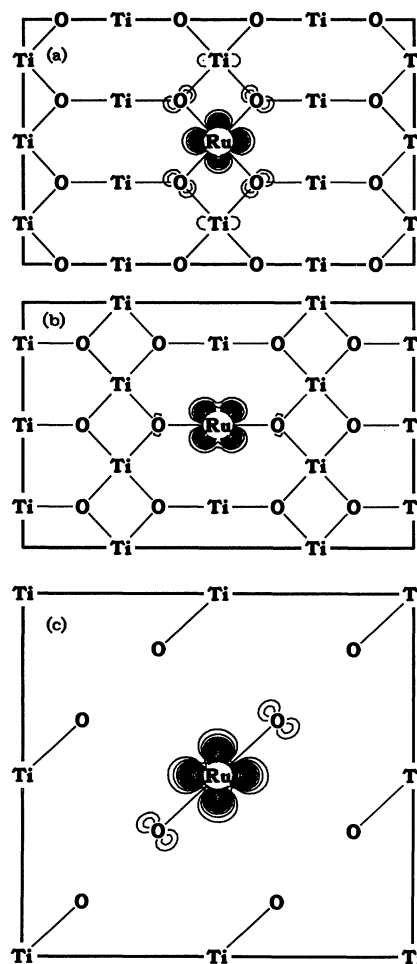


FIG. 3. Pseudo-charge-density plots for the three characteristic Ru-induced defect states for  $x = \frac{1}{24}$ , shown in symmetry planes revealing the Ru atomiclike  $d$  character. Panel (a) shows the (110) plane for the lowest band, panel (b) shows the second band in the  $(\bar{1}10)$  plane, and panel (c) shows the third defect band in the (001) plane. In each panel, the constant charge-density contours are separated by  $35 e/V_0$ , where  $V$  is the unit-cell volume.

ing to electron transfer from the top of the O 2*p* manifold to the lower edge of the Ti 3*d* states, while a 2-eV transition corresponds to electron transfer from the Ru 4*d* states to the lower edge of the Ti 3*d* states. Both experiments result in an ~1.2-eV separation between the top of the O 2*p* manifold to the narrow defect band, and are in good agreement with our theoretical predictions.

To determine the symmetry of the three defect states, we have calculated pseudocharge-density contour plots in high-symmetry planes of the tetragonal lattice for  $x = \frac{1}{24}$ , and these are shown in Fig. 3. We have indicated the Ti-O "bonding network" in the 2×2×3 supercell by solid lines, and have placed the single Ru impurity in the center of each plane. In panel (a), we show the (110) plane for the lowest band of  $d_{x^2-y^2}$ -like symmetry; panel (b) shows the second band in the (110) plane of  $d_{xy}$  symmetry; and panel (c) shows the third defect band in the (001) plane of  $d_{zx}$  symmetry. The symmetries of these states have been taken from the splitting of the five Ru atomic *d* states in the presence of an octahedron of O<sup>2-</sup> ions as the distortion from O<sub>h</sub> to D<sub>2h</sub> symmetry is small.<sup>2</sup>

From Fig. 3, it is clear that the three defect-induced gap states are localized on the Ru atoms, with a small amount of O 2*p* character associated with the  $pd\pi t_{2g}$  bonds occurring between the nearest-neighbor O<sup>2-</sup> ions.

To summarize, we have shown that Ru doping of TiO<sub>2</sub> results in three defect bands occurring in the fundamental gap. The character of these defect states has been determined from pseudo-charge-density plots to be localized atomiclike Ru 4*d* states of  $t_{2g}$ -like symmetry. The location of these defect states was found to be ~1 eV above the O 2*p* manifold, in agreement with experimental results. We show that good results may be obtained for the electronic structure of transition-metal dopants in ceramic oxides when the LDA is employed.

We would like to acknowledge N. Binggeli for useful discussions. This work was supported by the Division of Materials Research, Office of Basic Energy Sciences, U.S. Department of Energy, under Grant No. DE-FG02-89ER45391, and by the Minnesota Supercomputer Institute.

- 
- <sup>1</sup>K. M. Glassford and J. R. Chelikowsky, Phys. Rev. B **46**, 1284 (1992).
- <sup>2</sup>K. M. Glassford and J. R. Chelikowsky, Phys. Rev. B **47**, 1732 (1993).
- <sup>3</sup>N. Troullier and J. L. Martins, Phys. Rev. B **43**, 1993 (1991).
- <sup>4</sup>A. M. Rappe, K. M. Rabe, E. Kaxiras, and J. D. Joannopoulos, Phys. Rev. B **41**, 1227 (1990); D. Vanderbilt, *ibid.* **32**, 8412 (1985).
- <sup>5</sup>J. L. Martins and M. L. Cohen, Phys. Rev. B **37**, 6134 (1988); J. L. Martins, N. Troullier, and S.-H. Wei, *ibid.* **43**, 2213 (1990).
- <sup>6</sup>A. Fujishima and K. Honda, Bull. Chem. Soc. Jpn. **44**, 1148 (1971); Nature **238**, 37 (1972).
- <sup>7</sup>J. Manassen, D. Cahen, G. Hodes, and A. Sofer, Nature **263**, 97 (1976).
- <sup>8</sup>B. O'Regan and M. Grätzel, Nature **353**, 737 (1991).
- <sup>9</sup>F. Sabin, T. Türk, and A. Vogler, J. Photochem. Photobiol. A: Chem. **63**, 99 (1992).
- <sup>10</sup>Z. Luo and Q.-H. Gao, J. Photochem. Photobiol. A: Chem. **63**, 367 (1992).
- <sup>11</sup>K. R. Thampi, J. Kiwi, and M. Grätzel, Nature **327**, 506 (1987).
- <sup>12</sup>S. Trasatti and W. E. O'Grady, in *Advances in Electrochemistry and Electrochemical Engineering*, edited by H. Gerischer and C. W. Tobias (Wiley-Interscience, New York, 1981), Vol. 12, p. 177; S. Trasatti, Electrochim. Acta **36**, 225 (1991).
- <sup>13</sup>D. M. Novak, B. V. Tilak, and B. E. Conway, in *Modern Aspects of Electrochemistry*, edited by J. O'M. Bockris, B. E. Conway, and R. E. White (Plenum, New York, 1982), Vol. 14, p. 195.
- <sup>14</sup>J. Pascual, J. Camassel, and H. Mathieu, Phys. Rev. Lett. **39**, 1490 (1977); Phys. Rev. B **18**, 5606 (1978).
- <sup>15</sup>G. Lehmann and M. Taut, Phys. Status Solidi **54**, 469 (1972); O. Jepsen and O. K. Anderson, Solid State Commun. **9**, 1763 (1971).
- <sup>16</sup>K. Mizushima, M. Tanaka, A. Asai, S. Iida, and J. B. Goodenough, J. Phys. Chem. Solids **40**, 1129 (1979).
- <sup>17</sup>P. Triggs, F. Lévy, and F. E. Wagner, Mater. Res. Bull. **19**, 197 (1984).
- <sup>18</sup>P. Triggs, Helv. Phys. Acta **58**, 657 (1985).
- <sup>19</sup>N. Wagner and L. Kühnemund, Cryst. Res. Technol. **24**, 1009 (1989).
- <sup>20</sup>V. E. Henrich, G. Dresselhaus, and H. J. Zeiger, Phys. Rev. Lett. **36**, 1335 (1976); A. K. See and R. A. Bartynski, J. Vac. Sci. Technol. A **10**, 2591 (1992).
- <sup>21</sup>P. Triggs, H. Berger, C. A. Georg, and F. Lévy, Mater. Res. Bull. **18**, 677 (1983).
- <sup>22</sup>C. Gutiérrez and P. Salvador, J. Electroanal. Chem. **187**, 139 (1985).
- <sup>23</sup>Z. Zhang, S.-P. Jeng, and V. E. Henrich, Phys. Rev. B **43**, 12 004 (1991).
- <sup>24</sup>G. van der Laan, Phys. Rev. B **41**, 12 366 (1990).
- <sup>25</sup>J. Riga, C. Tenret-Noël, J. J. Pireaux, R. Caudano, J. J. Verbist, and Y. Gobillon, Phys. Scr. **16**, 351 (1977).